



Cite this: *Mater. Chem. Front.*, 2024, 8, 341

Received 1st June 2023,
Accepted 8th October 2023

DOI: 10.1039/d3qm00625e

rsc.li/frontiers-materials

Coupling electrochemical CO₂ reduction with value-added anodic oxidation reactions: progress and challenges

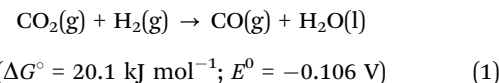
Yu Li and Tong-Bu Lu *

Converting CO₂ into chemicals using renewable electricity provides a promising avenue to realize carbon neutrality. Substituting the anodic oxygen evolution reaction by thermodynamically more favourable oxidation reactions with value-added products can significantly lower the cell voltage and enhance the output value of overall CO₂ electrolysis. In this review, we summarize the up-to-date breakthroughs in electrochemical systems featuring the CO₂ reduction reaction (CO₂RR) coupled with various anodic oxidation reactions. Moreover, major challenges with possible solutions and future prospects in this field are pointed out, which are expected to benefit researchers and propel this coupling strategy to industrial applications.

1. Introduction

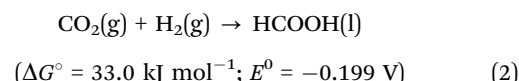
The global environmental issues and energy crisis are driving us to substitute traditional fossil fuels with green energy sources. Among the various emerging techniques, electrochemically converting CO₂ into value-added feedstocks can not only store renewable electricity in chemical bonds but also promote the natural carbon cycle, and therefore holds potential for realizing carbon-neutrality. Currently, great efforts have been devoted to developing efficient catalysts with excellent Faradaic efficiency (FE), high current density, and low overpotential for the electrochemical CO₂ reduction reaction (CO₂RR).^{1–4} However, although remarkable catalysts with near-unity FEs and close-to-zero overpotentials have emerged, energy utilization is still far from satisfactory considering the whole electrolysis. For instance, according to the Hess law, the energy consumption for CO₂ reduction to CO/HCOOH only takes a small part in the overall CO₂ electrolysis where the oxygen evolution reaction (OER) with a theoretical potential of 1.23 V *versus* reversible hydrogen electrode (vs. RHE) is usually adopted as the anodic reaction.

Cathode:

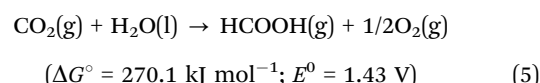
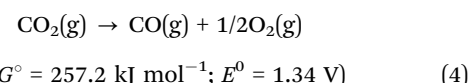
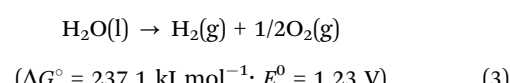


MOE International Joint Laboratory of Materials Microstructure, Institute for New Energy Materials and Low Carbon Technologies, School of Materials Science & Engineering, Tianjin University of Technology, Tianjin 300384, China.
E-mail: lutongbu@tjut.edu.cn

Anode:



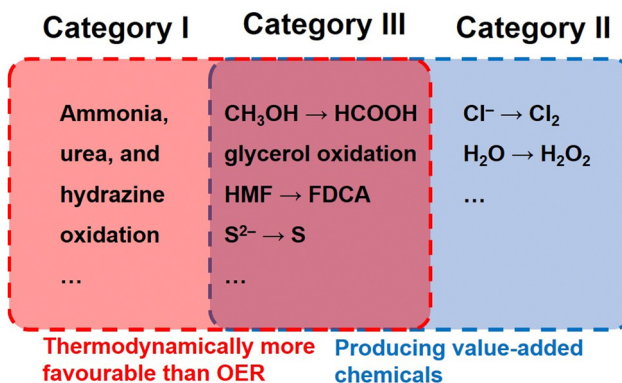
Overall:



Intuitively, the cathodic reduction of CO₂ to CO and HCOOH only takes 7.81% and 12.2% of the total energy consumption for overall CO₂ electrolysis, respectively, whereas the anodic OER consumes the vast majority of the electricity. In addition, the anodic product O₂ is of little value. To increase the energy utilization efficiency, many alternative reactions have been employed to replace the unsatisfactory OER (Table 1).^{5–9} Briefly, these reactions can be divided into three categories (Fig. 1). The first category includes reactions thermodynamically more favourable than the OER that can effectively reduce the cell voltage. For example, ammonia, urea and hydrazine oxidation reactions (denoted as the AOR, UOR, and HzOR, respectively) have been substituted for the OER in water splitting owing to their significantly lower theoretical potentials (0.06, 0.37 and

Table 1 Alternative anodic oxidation reactions for the OER in CO_2 overall electrolysis

	Anodic oxidation reaction	Redox potential (V vs. RHE)
OER	$\text{H}_2\text{O} \rightarrow \text{O}_2 + 4\text{H}^+ + 4\text{e}^-$	1.23
Category I	$2\text{NH}_3 + 6\text{OH}^- \rightarrow \text{N}_2 + 6\text{H}_2\text{O} + 6\text{e}^-$	0.06
	$\text{CO}(\text{NH}_2)_2 + 6\text{OH}^- \rightarrow \text{CO}_2 + \text{N}_2 + 5\text{H}_2\text{O} + 6\text{e}^-$	0.07
	$\text{N}_2\text{H}_4 + 4\text{OH}^- \rightarrow \text{N}_2 + 4\text{H}_2\text{O} + 4\text{e}^-$	-0.33
Category II	$2\text{Cl}^- \rightarrow \text{Cl}_2 + 2\text{e}^-$	1.36
	$2\text{H}_2\text{O} \rightarrow \text{H}_2\text{O}_2 + 2\text{H}^+ + 2\text{e}^-$	1.76
Category III	$\text{CH}_3\text{OH} + 3\text{OH}^- \rightarrow \text{HCOO}^- + 3\text{H}_2\text{O} + 2\text{e}^-$	0.11
	$\text{C}_3\text{H}_8\text{O}_3 + 11\text{OH}^- \rightarrow 3\text{HCOO}^- + 8\text{H}_2\text{O} + 8\text{e}^-$	0.14
	$\text{C}_6\text{H}_{12}\text{O}_6 + 2\text{OH}^- \rightarrow \text{C}_6\text{H}_{12}\text{O}_7 + \text{H}_2\text{O} + 2\text{e}^-$	0.90
	$\text{C}_6\text{H}_6\text{O}_3 + 6\text{OH}^- \rightarrow \text{C}_6\text{H}_2\text{O}_5^{2-} + 4\text{H}_2\text{O} + 4\text{e}^-$	0.30
	$\text{S}^{2-} \rightarrow \text{S} + 2\text{e}^-$	-0.48
	$2\text{HS}^- + 2\text{OH}^- \rightarrow \text{S}_2^{2-} + 2\text{H}_2\text{O} + 2\text{e}^-$	0.14

**Fig. 1** Different categories of alternative anodic oxidation reactions.

-0.33 V vs. RHE for the AOR, UOR, and HzOR, respectively) to markedly cut down the applied cell voltage.^{10–12} Although no value-added products are obtained, these sacrificial agent-like oxidation reactions can be adopted to eliminate pollutants in waste water.^{13,14}

Oxidation reactions featuring no superior theoretical potential but value-added products (Category II) have also been employed as the anodic side of full electrolysis. A representative is water oxidation to H_2O_2 ($2\text{H}_2\text{O} \rightarrow \text{H}_2\text{O}_2 + 2\text{H}^+ + 2\text{e}^-$, $E^\circ = 1.76$ V vs. RHE). Albeit this two-electron process requires

a higher potential by 0.53 V than that of the OER, the price of H_2O_2 (~\$560 per ton) is about 14 times as high as that of O_2 (~\$40 per ton), making this substitution economically viable.⁵ As the most attractive substitutions for the OER, selective oxidation of small organic molecules such as alcohols, aldehydes, and amines (Category III) enables simultaneous voltage reduction and value-added chemical production.^{15–20} The market prices of the raw materials and products for these alternative oxidation reactions are summarized in Table 2.⁵ Evidently, the added values and the electricity output (added value per electron) for the alternative oxidation reactions are all times higher than that for the OER. In particular, the conversion of 5-hydroxymethylfurfural (HMF) to 2,5-furandicarboxylic acid (FDCA) holds the highest added value of up to \$30970 per ton, suggesting its tremendous superiority compared with the OER.

Currently, increasing efforts are being devoted to coupling the above reactions with the CO_2 RR to fabricate an energy-efficient full electrolyser. Although several reviews on alternative anodic reactions coupled with the hydrogen evolution reaction (HER) have been reported, the case is much different in CO_2 electrolysis considering the electrolyte choice, mass transfer, electrode design, cell structure, *etc.*^{21–23} This review starts with a brief introduction of different types of anodic oxidation reactions. Subsequently, we will present up-to-date progress in alternative anodic reactions that have already been or hold the potential to be applied in CO_2 RR coupling systems, with elucidation of the structure–performance relationship. Finally, we will systematically discuss the challenges and prospects for CO_2 RR coupling systems regarding the design of electrocatalysts and electrolyzers for guidance on propelling this technique towards industrial applications.

2. Recent advances in coupling the CO_2 RR with alternative anodic reactions

2.1. Category I

N-containing species such as ammonia and urea are major pollutants in industrial and agricultural wastewater, the excessive emission of which will not only lead to the eutrophication

Table 2 Economic comparison between the OER and alternative oxidation reactions

Raw material	Market price of the raw material (\$ per ton)	Product	Market price of the product (\$ per ton)	Added value (\$ per ton)	Added value per electron (\$ per (ton e))
H_2O	0.6	O_2	40	39.4	9.8
H_2O	0.6	H_2O_2	560	559.4	279.7
NaCl	68	Cl_2	822	754	377
CH_3OH	340	HCOOH	970	630	157.5
$\text{CH}_3\text{CH}_2\text{OH}$	610	CH_3COOH	680	70	17.5
$\text{C}_3\text{H}_8\text{O}_3$ (glycerol)	970	$\text{C}_3\text{H}_6\text{O}_3$ (lactic acid)	1580	610	305
$\text{C}_5\text{H}_4\text{O}_2$ (furfural)	1170	$\text{C}_5\text{H}_4\text{O}_3$ (2-furoic acid)	6230	5060	2530
$\text{C}_6\text{H}_6\text{O}_3$ (5-Hydroxymethylfurfural)	1030	$\text{C}_6\text{H}_4\text{O}_5$ (2,5-Furandicarboxylic acid)	32000	30970	5161.7
$\text{C}_6\text{H}_{12}\text{O}_6$ (glucose)	315	$\text{C}_6\text{H}_{12}\text{O}_7$ (gluconic acid)	644	329	164.5

of water and destroy the river and lake ecosystems, but also threaten drinking water safety. Classical methods to decompose these pollutants are based on chemical oxidation reactions using toxic and hazardous reagents, which are not preferred given the increasing environmental and economic requirements. Electrochemical oxidation of N-containing pollutants provides appealing routes to remedy the above issues. The pollutants can be transformed directly by current on the electrode surface or indirectly by active radicals *in situ* generated during electrolysis, rather than hazardous chemicals. However, in spite of their low theoretical potentials, both the AOR and UOR involve $6e^-$ -transfer processes ($2\text{NH}_3 + 6\text{OH}^- \rightarrow \text{N}_2 + 6\text{H}_2\text{O} + 6e^-$; $\text{CO}(\text{NH}_2)_2 + 6\text{OH}^- \rightarrow \text{CO}_2 + \text{N}_2 + 5\text{H}_2\text{O} + 6e^-$), and thus suffer from sluggish kinetics. Accordingly, developing highly efficient catalysts is essential for the energy-efficient $\text{CO}_2\text{RR-AOR}$ and $\text{CO}_2\text{RR-UOR}$ couple at an industrial current density ($> 100 \text{ mA cm}^{-2}$).

According to the dehydrogenation degree of N intermediates in the N–N coupling step, there are two possible pathways for AOR: (1) the adsorbed ammonia undergoes continuous dehydrogenation steps and the N–N coupling step occurs between two $^*\text{N}$ species; (2) the N–N coupling step occurs between two incomplete dehydrogenated $^*\text{NH}_x$ species followed by further dehydrogenation of $^*\text{N}_2\text{H}_y$ species ($x = 1\text{--}3$ and $y = 2\text{--}5$).^{24–26} Pt-based catalysts have shown excellent activity in the AOR. The introduction of Ir and Ni into the Pt lattice can decrease the energy barrier of dehydrogenation of $^*\text{NH}_2$ to $^*\text{NH}$ and the rate-determining step (RDS) on the Pt surface *via* elevating the d-band centre for enhanced $^*\text{NH}$ adsorption, thereby accelerating the reaction kinetics and reducing the overpotential.^{25,26} Recently, Ni catalysts have been investigated for the cost-effective AOR. Xu *et al.* reported a bimetallic NiCu catalyst that could achieve 80% removal of ammonia in 500 ppm NH_3 solution.²⁷ Almomani *et al.* reported that an *in situ* formed $\text{Ni}(\text{OH})_2$ layer over NiO endowed the NiO-TiO_2 composite catalyst with over 90% removal of N in wastewater with a low ammonia concentration of $< 100 \text{ ppm}$.²⁸

Although inspiring progress has been made in the AOR, the development of $\text{CO}_2\text{RR-AOR}$ full electrolysis remains immature. Klinkova's group evaluated the $\text{CO}_2\text{RR-AOR}$ couple featuring an Ag/C cathode and Pt/C anode in an H-type cell.²⁹ Compared with the $\text{CO}_2\text{RR-OER}$, the cell voltage decreased by 0.78 V at a current density (j) of 0.1 mA cm^{-2} with the addition of 1 M ammonia in the anolyte. However, the improvement shrank to 0.32 V when j was increased to 10 mA cm^{-2} . Besides, the Pt/C catalyst got poisoned easily due to the overstrong adsorption of $^*\text{N}$ -species, and showed no activity towards the AOR after a four-hour test.

As shown above, in addition to the low solubility of CO_2 in aqueous solution ($\sim 34 \text{ mM}$ under ambient conditions), the poor mass transfer efficiency over both the anode and the cathode in commonly used H-type cells heavily hindered the electrocatalytic performance of the $\text{CO}_2\text{RR-AOR}$ couple. To overcome the mass transfer limitation, a flow cell with a cathodic gas diffusion electrode (GDE) was fabricated. Both the anolyte and catholyte flow in the flow field immediately remove

the products and refresh the electrolyte near the electrode, thereby exposing active sites with a high-concentration of local ammonia and CO_2 . Moreover, the cathodic GDE helps to construct a three-phase interface composed of electrode–water– CO_2 , which prominently enhances the contact between the catalyst and CO_2 and thus boosts the current density (a more detailed discussion is presented in Section 3.2). Choi *et al.* successfully coupled the CO_2RR with the AOR in a closely packed gas diffusion electrolyser consisting of a Au cathode and a Pt/C anode (Fig. 2a).³⁰ The cell voltages of the $\text{CO}_2\text{RR-OER}$ and $\text{CO}_2\text{RR-AOR}$ were 3.0 and 2.0 V at 10 mA cm^{-2} , respectively, and the disparity increased to 1.5 V at 50 mA cm^{-2} , demonstrating the boosted energy efficiency for the $\text{CO}_2\text{RR-AOR}$ couple in a gas diffusion electrolyser (Fig. 2b). Moreover, the H_2/CO ratio of the cathodic product syngas could be optimized by changing the NH_3 concentration in the anolyte (Fig. 2c). However, a similar activity decrease was also observed for anodic Pt/C in this work. In addition, it should be pointed out that these reported $\text{CO}_2\text{RR-AOR}$ couples require an extremely high concentration of ammonia to markedly reduce the full cell voltage, whereas the concentration of NH_3 (calculated by N mass) in domestic or agricultural effluents is usually below 100 mg L^{-1} , equal to approximately 7 mM NH_3 , which means that extra NH_3 enrichment procedures are demanded for the wastewater before being applied in the $\text{CO}_2\text{RR-AOR}$ couple. Therefore, highly active catalysts that can efficiently convert low concentrations of NH_3 with a prolonged lifetime are crucial for the utilization of the $\text{CO}_2\text{RR-AOR}$ technique.

For the UOR, apart from the dehydrogenation N–N coupling steps, it also involves the breakage of the C–N bond before the formation of N_2 .³¹ Jiang *et al.* found that on O-incorporated NiMoP nanotube arrays, the last dehydrogenation step from $^*\text{CONHN}$ to $^*\text{CON}_2$ and subsequent C–N dissociation of $^*\text{CON}_2$ into $^*\text{CO}$ and N_2 were the slow steps for the UOR, whereas the

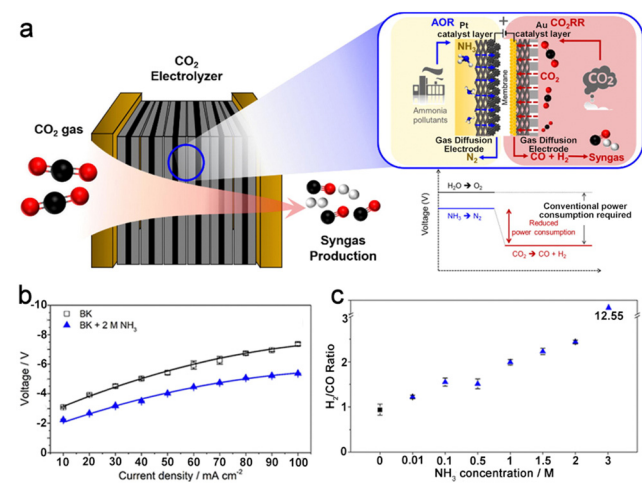


Fig. 2 (a) Schematic illustration of the $\text{CO}_2\text{RR-AOR}$ couple in a gas diffusion electrolyser. (b) Voltages at different current densities in 0.5 M KHCO_3 (BK) or 0.5 M $\text{KHCO}_3 + 2 \text{ M NH}_3$ (BK + 2 M NH_3). (c) H_2/CO ratio of syngas as a function of the NH_3 concentration at 10 mA cm^{-2} . Reproduced with permission from ref. 30. Copyright 2022, Elsevier Ltd.

other steps were all spontaneous.¹² In an electrolyte containing 1.0 M KOH + 0.5 M urea, a potential of merely 1.41 V vs. RHE was required to deliver a *j* value of 100 mA cm⁻², 340 mV lower than that of the OER, indicating the improved energy efficiency for the UOR. Besides, the result of long-term electrolysis revealed that the current density slightly dropped from 20 to 17.5 mA cm⁻² after 40 h of the UOR, implying the fine stability of the catalyst. Recently, Clark *et al.* investigated the feasibility of coupling the CO₂RR with the UOR using Sn wire and a NiFe film as corresponding electrodes.³² The voltage of the full electrolyser was reduced by the addition of 0.25 M urea in the anolyte, and the FE of the CO₂RR was even slightly higher than that of CO₂ coupled with the OER.

Hydrazine is also a pollutant in wastewater, and many efforts have been devoted to the development of efficient HzOR catalysts. HzOR involves 4-e⁻ transfer with extremely low theoretical potential (N₂H₄ + 4OH⁻ → N₂ + 4H₂O + 4e⁻; *E*⁰ = -0.33 V vs. RHE), which is beneficial to reduce the full cell voltage when employed as the anode reaction. Zhu *et al.* fabricated a Ni/C hybrid nanosheet array catalyst for efficient HzOR.¹⁰ DFT calculation results revealed that the Ni sites in the hybrid catalyst favoured the dehydrogenation of N₂H₄ to N₂, thereby enhancing the HzOR performance. Shi's group reported an unusual HzOR pathway on the CoP/NiCoP heterogenous interface featuring the cleavage of the N-N bond before dehydrogenation with a reduced energy barrier.¹¹ As a result, a potential of merely 0.09 V vs. RHE was required to deliver 200 mA cm⁻² current density for HzOR by the optimized catalyst in 1.0 M KOH + 0.1 M N₂H₄, 1.54 V lower than that for OER by RuO₂. However, the CO₂RR-HzOR couple has not been reported, to our knowledge. In fact, we can only find limited literature that has reported the successful coupling of the CO₂RR with the above water pollutant degradation reactions, whereas the latter have already been employed to couple with the hydrogen evolution reaction (HER). The main reason is that the CO₂RR performance is closely influenced by the catalyst activity, gas-liquid-solid interfacial mass transfer, electrolyte types, *etc.*, much more complicated than the case of water splitting. Moreover, the requirement of high concentrations of pollutants to significantly reduce the full cell voltage leads to extra energy-consuming preconcentration of wastewater. Accordingly, further techno-economic analysis is required to evaluate the coupling of the CO₂RR with Category I reactions, and developing highly active catalysts that can deal with low concentrations (ppm level) of pollutants may address the issue.

2.2. Category II

The chlorine oxidation reaction (COR) is one of the most crucial chemical industrial techniques as the products Cl₂ and ClO⁻ are important feedstocks in the pharmacy, disinfection, and rubber industries. Coupling CO₂ reduction to CO with the COR enables simultaneous production of CO, KHCO₃, and Cl₂ with 100% atom economy theoretically (3CO₂ + 2KCl + H₂O → CO + 2KHCO₃ + Cl₂). For example, Guo *et al.* have successfully assembled a carbon black supported Ni catalyst cathode and

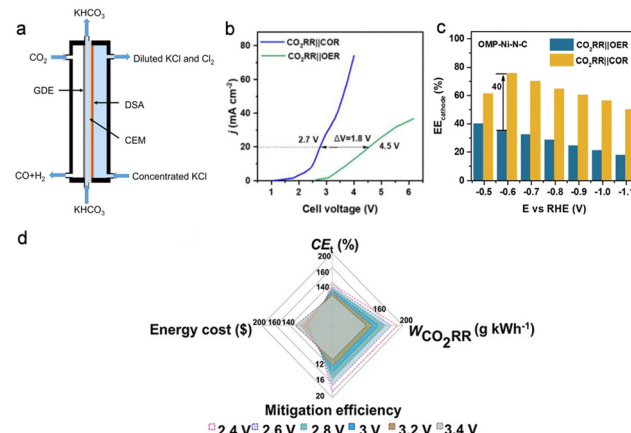


Fig. 3 (a) Schematic illustration of the flow cell for the CO₂RR-COR couple. Reproduced with permission from ref. 33. Copyright 2020, Elsevier Ltd. (b) Linear sweep voltammetry curves and (c) cathode energy efficiencies for the CO₂RR coupled with the COR or OER. Reproduced with permission from ref. 34. Copyright 2022, Elsevier Ltd. (d) CO₂ emission and economy evaluation *via* total cell efficiency, mitigation efficiency, the weight of CO₂ reduced per kWh electricity consumption, and energy cost on the basis of per kWh electricity consumption for the CO₂RR-COR couple in seawater. Reproduced with permission from ref. 35. Copyright 2021, John Wiley & Sons, Inc.

commercial dimensional stable anode in a gas diffusion electrolyser for the efficient CO₂RR-COR (Fig. 3a).³³ High FEs of up to 98.5% and 75.2% were achieved at 250 mA cm⁻² for CO₂RR-to-CO and COR-to-Cl₂, respectively. Lu's group introduced ordered mesoporous structures into cathodic Ni-N-C and anodic Co₃O₄ catalysts to enhance the activity of the CO₂RR-COR couple.³⁴ The improved mass transfer owing to the ordered mesoporous structure effectively boosted the current density. Moreover, the cell voltage was sharply reduced from 4.5 to 2.7 V to achieve 20 mA cm⁻² with the substitution of the OER with the COR (Fig. 3b), and the energy efficiency (EE) for the cathode was increased by 40% (Fig. 3c). Qiu's group have evaluated the economy and the net reduction of CO₂ for the CO₂RR-COR using seawater as the electrolyte, and the results suggested a total cell efficiency for producing CO and Cl₂ exceeding 100% without extra CO₂ emission (Fig. 3d).³⁵ The above work demonstrates the huge potential and viability of the sCO₂RR-COR couple in the industrial process.

H₂O oxidation to H₂O₂ rather than O₂ is attracting increasing interest. Although the theoretical potential for H₂O₂ formation (1.76 V vs. RHE) is higher than that of O₂ (1.23 V vs. RHE), 2-e⁻ transfer of the H₂O₂ evolution reaction makes it more dynamically favoured than the OER. However, no work has been reported focused on coupling the CO₂RR with the H₂O₂ evolution reaction to date. The Wang group found a CO₂/carbonate mediated electrochemical H₂O oxidation for high-performance H₂O₂ production.³⁶ The carbonate ions could steer the 4-e⁻ pathway to 2-e⁻ through carbonate radicals and percarbonate intermediates. Consequently, an industrial scale current density of up to 1.3 A cm⁻² was achieved with an H₂O₂ FE of 70% in the K₂CO₃ electrolyte. This inspiring result

indicates the possibility of coupling the CO₂RR with H₂O oxidation to H₂O₂ in the anion exchange membrane (AEM) electrolyser where *in situ* formed CO₃²⁻ in the cathode can migrate to the anode to help boost the formation of H₂O₂.

2.3. Category III

Methanol is a main product in methane conversion and an important building block for the chemical industry. Selective oxidation of methanol to formic acid (formate) is desired given the large disparity in prices of methanol (~\$200 per ton) and formic acid (~\$600 per ton). Wei *et al.* fabricated CuO nanosheets on Cu foam for the efficient methanol oxidation reaction (MOR) (Fig. 4a).¹⁶ A high FE_{formate} of up to 95% was achieved for the MOR, and the potential was decreased by 250 mV to achieve a current density of 10 mA cm⁻² compared with that for the OER. Besides, mesoporous SnO₂ on carbon cloth was prepared for the efficient CO₂RR with 81% FE_{formate}. For the CO₂RR-MOR couple, it required only 0.93 V to deliver a current density of 10 mA cm⁻², which was 500 mV lower than that for the CO₂RR-OER. Another work by Cao *et al.* presented a CO₂RR-MOR full electrolyser equipped with Bi- and Ni-metal-organic framework-derived catalysts as the respective cathode

and anode.¹⁷ A current density of 27 mA cm⁻² was achieved at a cell voltage of 3.0 V with a FE_{formate} of ~100% at both electrodes (Fig. 4b). Lan's group successfully integrated metalloporphyrin (Ni) and Ni₈ clusters in PCN-601 as a bifunctional electrocatalyst for the CO₂RR-MOR couple.³⁷ The Ni site in metalloporphyrin served as the active centre for the CO₂RR to CO, while the Ni₈ cluster acted as the site for the MOR to formate. Consequently, high FE_{CO} and FE_{formate} values of over 90% were obtained at 2.2 V with a current density of 7 mA cm⁻². Nevertheless, the current densities above are too low to meet industrial requirements. Recently, our group developed a bifunctional CuSn alloy electrocatalyst with a hierarchical structure for the CO₂RR-MOR couple at a high current density.¹⁵ In an H-type cell, the CO₂RR-MOR couple delivered a current density as high as 125 mA cm⁻² with near-unity FE_{formate} at both sides, corresponding to a formate production rate of up to 3313 μmol h⁻¹ cm⁻². Such a strategy contributed to a reduction in energy consumption by 40% for formate synthesis. Moreover, *in situ* Raman spectroscopic results revealed that the CH₃OH adsorbed on the catalyst surface *via* an O atom followed by a series of dehydrogenation steps to form an *OCH intermediate. Subsequently, *OCHO was generated through the addition of an O atom from the OH group to *OCH and then desorbed from the CuSn alloy surface for formate formation (Fig. 4c and d). This reaction pathway was also verified on partially pyrolyzed Ni-organic frameworks.¹⁸ The *in situ* formed NiOOH sites were conducive to O-H activation and thus promote the oxidation of methanol to formate. In a zero-gap membrane electrode assembly (MEA), the CO₂RR-MOR couple exhibited an excellent performance of ~500 mA cm⁻² at 2.2 V with over 90% FEs for both CO₂RR-to-CO and MOR-to-formate, ranking top among the up-to-date CO₂RR-MOR systems (Fig. 4e and f).

Electrochemical upgrade of biomass-derived materials such as glycerol, furfural and glucose into useful chemicals is thermodynamically more favourable than the OER owing to the -CHO and -OH groups. Glycerol is a massive byproduct of the transesterification process for biodiesel and soap production, and it is profitable to upgrade glycerol into other chemicals through the glycerol oxidation reaction (GOR). Verma *et al.* performed a techno-economic analysis of cradle-to-gate CO₂ emissions of the overall CO₂RR process using grid electricity, and the result indicated that only HCOOH could be produced in a carbon-neutral or -negative manner when the OER was employed as the anodic reaction.³⁸ As a step further, they found that using the GOR on Pt black at the anode lowered the onset potential for the overall CO₂ electrolysis by 0.85 V, contributing to an energy consumption reduction of 53%, which drastically reduced the operating costs and carbon footprint of CO₂ electrolysis and thereby made the production of CO, C₂H₄, and CH₃CH₂OH become carbon-neutral, strongly evidencing the economic viability of the CO₂RR-GOR couple. However, there are various products for the GOR such as glyceraldehyde, glycerate, lactate, glycolate, formate, and carbonate, resulting in poor selectivity. A flow cell consisting of a Bi/C cathode and Pt/C anode has been reported for coupling the CO₂RR with

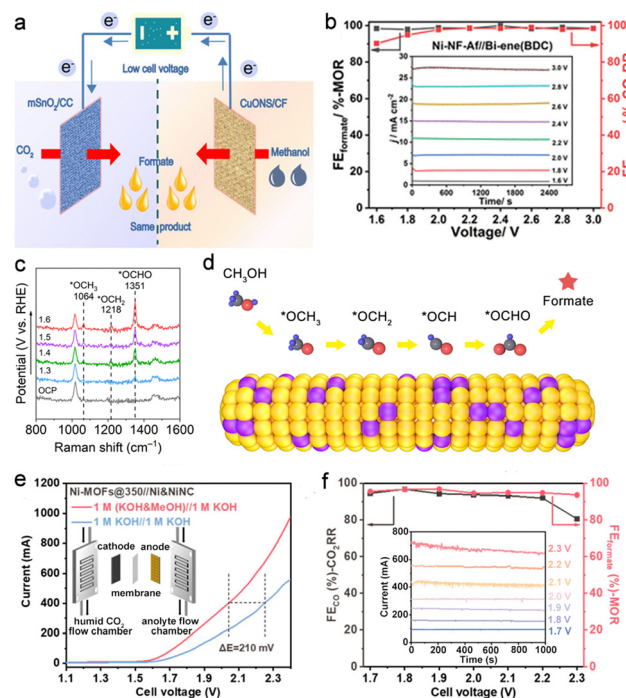


Fig. 4 (a) Schematic illustration of the CO₂RR-MOR couple. Reproduced with permission from ref. 16. Copyright 2020, John Wiley & Sons, Inc. (b) Cathodic and anodic FE_{formate} of the CO₂RR-MOR couple using Bi- and Ni-MOF-derived materials as corresponding electrodes. Reproduced with permission from ref. 17. Copyright 2021, John Wiley & Sons, Inc. (c) *In situ* Raman spectra and the (d) proposed reaction pathway for the MOR on CuSn alloy. Reproduced with permission from ref. 15. Copyright 2022, Elsevier Ltd. (e) Polarization curves (inset shows the MEA scheme) and (f) voltage-dependent FE (inset shows the corresponding *i*-*t* curves) for the CO₂RR-MOR in an MEA electrolyser. Reproduced with permission from ref. 18. Copyright 2023, American Chemical Society.

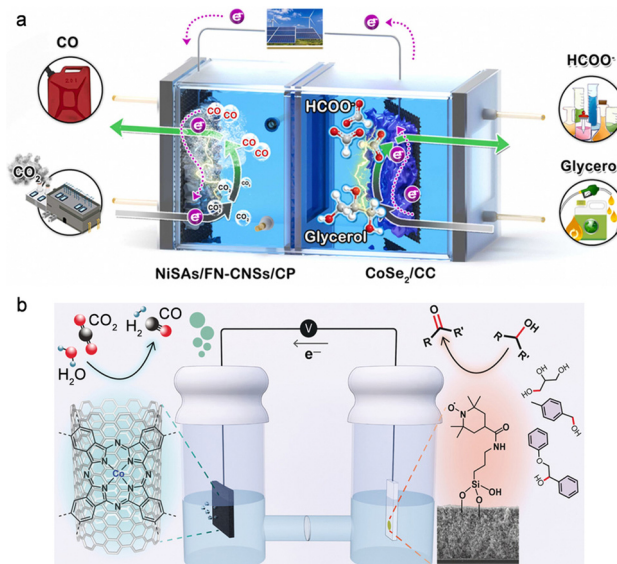


Fig. 5 (a) Schematic illustration of the electrolyser featuring CO₂RR-to-CO coupled with GOR-to-formate. Reproduced with permission from ref. 40. Copyright 2022, Elsevier Ltd. (b) Coproduction of syngas and glycer-aldehyde using the CO₂RR-GOR couple. Reproduced with permission from ref. 41. Copyright 2020, John Wiley & Sons, Inc.

the GOR.³⁹ While a high formate concentration of 18 g L⁻¹ was obtained by the cathodic CO₂RR with over 80% FE at 200 mA cm⁻², a low FE of ~20% was delivered for formate by the anodic GOR owing to the severe overoxidation evidenced by the high FE of up to 40% for the carbonate product. Wang *et al.* constructed an F, N co-doped carbon nanosheet-supported Ni single atom cathode and carbon cloth-supported CoSe₂ anode to couple the CO₂RR with the GOR (Fig. 5a).⁴⁰ A long-term continuous electrolysis of 400 h was achieved at 100 mA cm⁻² with both the cathodic FE_{CO} and anodic FE_{formate} kept over 90%. Apart from formate, another useful chemical glyceraldehyde was selectively generated at the anode of the CO₂RR-GOR by Reisner's group.⁴¹ They reported a hybrid assembly based on a (2,2,6,6-tetramethylpiperidin-1-yl)oxyl electrocatalyst modified with a silatrane-anchor for selective glyceraldehyde production from glycerol with an FE of up to 83%; meanwhile, syngas was produced at the cathode using cobalt phthalocyanine on carbon nanotubes as the catalyst (Fig. 5b).

The electrochemical 5-hydroxymethylfurfural (HMF) oxidation reaction (HMFOR) has attracted increasing attention.⁴²⁻⁴⁵ Composed of a -CHO and a -CH₂OH with a furan ring, HMF can be oxidized to 2,5-diformylfuran (DFF) *via* initial -CH₂OH oxidation, or 5-hydroxymethyl-2-furancarboxylic acid (HMFCA) *via* initial -CHO oxidation. Subsequently, the DFF and HMFCA can be further oxidized to 2-formyl-5-furancarboxylic acid (FFCA), and finally to 2,5-furandicarboxylic acid (FDCA) (Fig. 6). The choice of the DFF-pathway or HMFCA-pathway for the oxidation of HMF to FDCA greatly depends on the pH of the electrolyte.⁴⁶ Generally, the HMFOR undergoes the HMFCA-path in a strong alkaline electrolyte (pH > 13) due to the

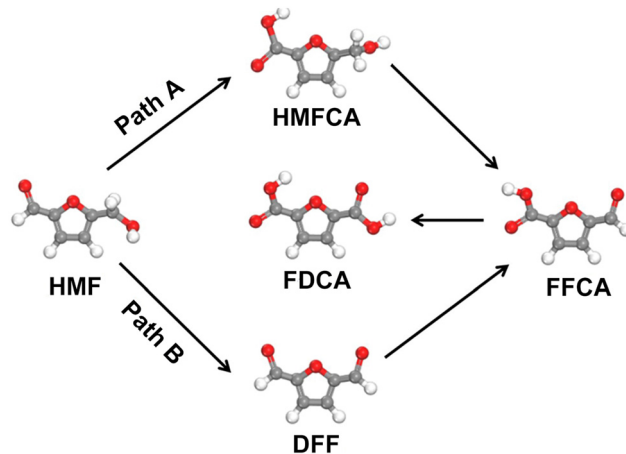


Fig. 6 Reaction pathways for the HMFOR.

preferential adsorption of the aldehyde group on the catalyst, whereas the DFF-pathway is favoured in the electrolyte with pH < 13 where the adsorption of the alcohol group becomes thermodynamically more favourable.⁴⁶ To further investigate the HMFOR pathway, Wang's group developed a vibrational spectroscopy technique using *in situ* sum frequency generation to monitor the interfacial process during the HMFOR.⁴⁷ A signal related to HMFCA emerged and grew stronger as the electrolysis time was prolonged, which validated the HMFCA-pathway for the HMFOR. To simultaneously promote the oxidation of -CH₂OH and -CHO, Lu *et al.* introduced Ni into the tetrahedral catalytic sites of cobalt spinel oxides.⁴⁸ The Ni and Co sites served as active centres for -CH₂OH and -CHO adsorption, respectively, thus enhancing the HMFOR with a high yield of 92.4% and FE of 90.3% for FDCA.

With the remarkable progress made in the HMFOR, however, few works about the CO₂RR-HMFOR couple have been reported so far. Recently, Han's group carried out the coupling of the HMFOR with the CO₂RR (Fig. 7a and b).¹⁹ The full electrolyser featuring PdO_x/ZIF-8 as the cathode and PdO as the anode only required an onset cell voltage of 1.06 V for the CO₂RR-HMFOR couple, 0.71 V lower than that of the CO₂RR-OER couple (Fig. 7c). Different from previous studies for the HMFOR, an acidic anolyte containing H₂SO₄ (0.5 M)/CH₃CN (6.0 M)/H₂O was employed, and the products were mainly maleic acid and formic acid, indicating that a strong acidic environment may lead to an unconventional reaction pathway involving C-C breaking and furan ring opening for the HMFOR. Notably, the organic acid yield reached 84.3% for the HMFOR, including 60.0% formic acid and 24.3% maleic acid, accompanied by a FE_{CO} of 97.0% for the CO₂RR at 103.5 mA cm⁻² (Fig. 7d and e).

There are also some other oxidation reactions that have already been or have the potential to be coupled with the CO₂RR. Sulfur production through the sulfide oxidation reaction (SOR) is an appealing candidate for the anodic reaction in overall CO₂ electrolysis by virtue of its low potential (0.14 V vs. RHE). Besides, the ingredient H₂S/S²⁻ widely exists in industrial exhaust/effluent. Therefore, coupling the CO₂RR with the

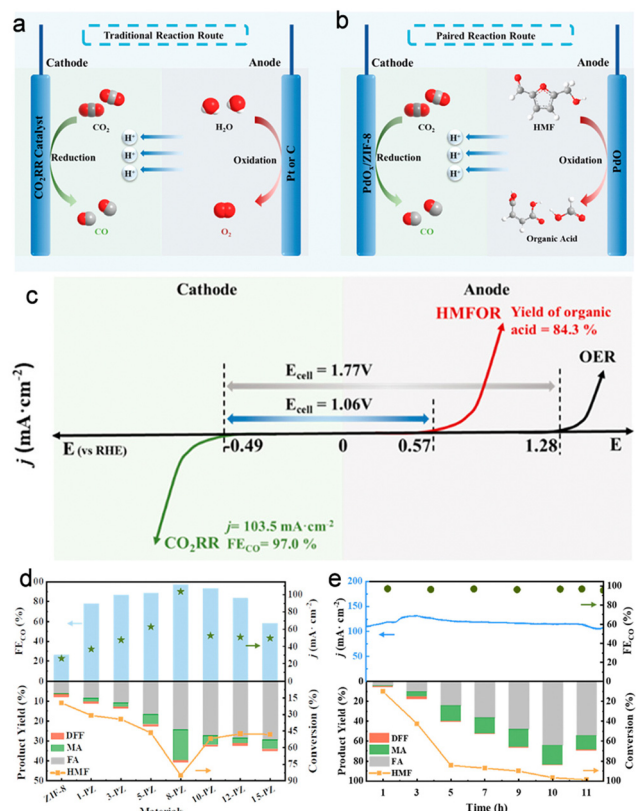


Fig. 7 Overview of (a) CO₂RR-OER and (b) CO₂RR-HMFOR routes. (c) Comparison between the CO₂RR-OER and the CO₂RR-HMFOR. (d) CO₂RR and HMFOR performances with different anodic catalysts. (e) Long-term electrolysis results of the CO₂RR and HMFOR. Reproduced with permission from ref. 19. Copyright 2022, American Chemical Society.

SOR is also of environmental value. Liu's group recently carried out a co-electrolysis system consisting of Bi for CO₂RR-to-formate, and S, Cu-codoped cobalt hydroxide for SOR-to-sulfur, which showed a pronounced reduction in energy consumption.⁴⁹ To avoid the deposition of S on the anode, an alkaline electrolyte (1 M KOH + 1 M K₂S) was employed to generate soluble S_x²⁻ from the direct SOR. As a result, the substitution of the OER with the SOR markedly lowered the cell voltage from 3.43 to 2.10 V at 100 mA cm⁻², with near-unity faradaic efficiencies for both sides. Economic evaluation based on the cell operation conditions and the prices of cathodic and anodic products revealed a gross margin of \$0.35 kW h⁻¹ for the CO₂RR-SOR, about 2 times as high as that for the CO₂RR-OER (\$0.18 kW h⁻¹), further demonstrating the economic viability of the former. Electricity-driven partial oxidation of methane is also a promising anodic reaction of overall CO₂ electrolysis.^{50,51} Lu *et al.* developed an efficient solid oxide electrolyser for the coupling of CO₂ reduction with CH₄ oxidation to produce syngas.⁵² However, the high operating temperature (1073 K) for O²⁻ transport led to extra energy input. Given the insoluble CH₄, the construction of a high-quality gas-liquid-solid interface using gas diffusion electrodes will favour the efficient coupling of the CO₂RR with CH₄ oxidation. In addition to the aforementioned small molecule oxidation,

electrochemical upcycling of plastic waste⁵³ or reforming of raw biomass such as lignin⁵⁴ and chitin⁵⁵ are also competing substitutions for the OER. In particular, electrochemical conversions of lignin and chitin have already been successfully employed as the anodic reaction for energy-saving hydrogen evolution systems, demonstrating the possibility for CO₂ electrolysis.^{55,56} However, achieving high selectivity for the target product remains a huge challenge due to the complicated structures and decomposition pathways for these macromolecules. Moreover, in addition to the electrolysis device design, comprehensive techno-economic analysis covering not only the design of electrolysis devices but also the up- and down-stream supply chain is urgently demanded for guidance on the development of industrial-scale plants.

3. Challenges in coupling the CO₂RR with alternative anodic reactions

3.1. Trade-off between conversion and current density

To reduce the cell voltage and enhance the current density for overall CO₂ electrolysis, a high-concentration substrate is usually required on the anodic side. However, the concentration of the substrate decreases as the electrolysis time is prolonged, which leads to a continuous drop in current density. Besides, the faradaic efficiencies of these alternative anodic reactions may also decrease due to the low reactant concentration. To address this issue, one common way is to refresh the anolyte with a high-concentration substrate.¹⁵ However, such a strategy heavily restricts the conversion of the substrate, and brings extra procedures for the separation of products and the unreacted substrate. A more feasible solution is to develop efficient catalysts that are able to selectively convert the substrates at low concentrations. Wang's group fabricated a catalyst featuring dispersed Ru atoms in a Cu nanowire matrix towards efficient NO₃⁻ reduction to NH₃.⁵⁷ An industrial-scale current density of up to 1 A cm⁻² was achieved with an NH₃ FE of 93% at a low nitrate concentration of typical industrial wastewater (2000 ppm). More importantly, 99% of the nitrate could be converted to NH₃ with the FE maintained over 90% at 400 mA cm⁻², with the concentration of the nitrate residue as low as 50 ppm. Although this work is focused on the cathodic process, we can learn from it that active sites with a high density (dispersed Ru atoms) and porous structure with a high surface area (hollow Cu nanowire matrix) endow the catalyst with enhanced performance at a low substrate concentration. Besides, increasing the local substrate concentration near the electrode surface with functional groups may also help to maintain the faradaic efficiency and current density when the substrate concentration is reduced. For example, amine groups anchored on the electrode surface can capture dilute CO₂ and thus enhance the FE for the CO₂RR.^{58,59}

3.2. Electrolyser design

In addition to electrocatalysts, electrolyzers with different architectures also influence the performance of overall CO₂

electrolysis.^{60,61} H-type cells are widely employed in various electrochemical reactions due to their simple and cost-effective setup. However, the low CO_2 solubility in aqueous solution ($\sim 34 \text{ mM}$ under ambient conditions) and the slow CO_2 diffusion limit the mass transfer efficiency over the electrode, leading to inferior current density. Moreover, the excessive supply of H_2O and insufficient supply of CO_2 over the immersed electrode are unfavoured for the sCO_2RR to multi-carbon products (denoted as C_{2+} , *i.e.*, C_2H_4 and $\text{C}_2\text{H}_5\text{OH}$) as high concentrations of CO_2 or CO intermediates are preferred for the C-C coupling process.^{62–64} Besides, the long distance between the anode and the cathode inevitably results in a pronounced voltage drop due to the high resistance.

Compared with H-type cells, flow cells enable efficient mass-transfer for industrial-scale current density owing to the high-quality catalyst-electrolyte-gas tri-phase interface and the continuous electrolyte/gas flow (Fig. 8a).⁶⁵ Different from H-type cells, a gas diffusion electrode consisting of a hydrophobic gas

diffusion layer (GDL) and catalyst layer is required. Gaseous CO_2 can efficiently diffuse across the GDL to the catalyst layer to meet the catholyte, thereby forming the above-mentioned tri-phase interface for the enhanced CO_2RR . The flowing anolyte also promotes the removal of products and attached bubbles and facilitates mass transfer near the anode, thereby enhancing the anodic reaction rate. However, flow cells also show drawbacks. The hydrophobic surface of the GDE gradually becomes hydrophilic during high-current electrolysis, which leads to catholyte flooding and gas feed blocking. Besides, the commonly used carbon paper to fabricate GDL is broken easily in the electrolyte/gas flow due to its weak mechanical strength. To alleviate these issues, Dinh *et al.* reported a polytetrafluoroethylene (PTFE)/Cu/carbon nanoparticles/graphite composite GDE which could run for 150 h with the C_2H_4 FE maintained over 60%.⁶⁴ In sharp contrast, the C_2H_4 FE rapidly dropped to 10% within 1 h for the conventional carbon paper/Cu GDE. The robust PTFE with a hydrophobic surface effectively prevented flooding, and the carbon nanoparticles and graphite layer stabilized the Cu catalyst surface.

A catholyte-free MEA electrolyser provides a solution to prevent the flooding issue (Fig. 8b).^{65,66} Moreover, the closely packed cathode-membrane-anode structure of the MEA minimizes the electricity resistance for enhanced energy efficiency. Zhou *et al.* reported that in a flow cell, the CO_2RR -MOR required 2.74 V to deliver a current density of 100 mA cm^{-2} , whereas a high current density approaching 500 mA cm^{-2} was achieved at merely 2.4 V in an MEA electrolyser.¹⁸ This is especially important for a scale-up stack where several MEAs are integrated. An electrolyser stack with four $10 \times 10 \text{ cm}^2$ MEAs was successfully constructed for scale-up CO_2 electrolysis by Bao's group (Fig. 8c).⁶⁷ Impressively, a current of 60 A was achieved with a C_{2+} FE of over 80% at a cell voltage of $\sim 13.5 \text{ V}$, and the current could be further increased to 150 A with nearly 90% C_{2+} FE at a cell voltage less than 11 V when fed with CO. Such a scale-up device provides an appealing way for practical utilization of CO_2 electrolysis, and further improvements are required to couple the CO_2RR with various value-added anodic reactions in the future.

In addition to the electrolyser architecture, the electrolyte also plays a pivotal role in electrolysis. An alkaline solution is employed in many CO_2RR cases owing to the low ohmic resistance and effective suppression of the HER. However, severe CO_2 loss (75–95%) occurs under these conditions due to the rapid reaction of CO_2 with alkali to form carbonate and bicarbonate (Fig. 9), and the regeneration of the alkaline electrolyte accounts for 60–75% of total energy consumption.⁶⁵ Moreover, CO_2RR products such as formate can diffuse across the anion exchange membrane to the anodic part, leading to difficulties in product collection and separation. Therefore, the acidic CO_2RR seems attractive. Unfortunately, most of the alternative anodic reactions such as CH_3OH , glycerol, and HMF oxidation are kinetically favourable in alkaline electrolytes. To deal with the above issues, a bipolar membrane was adopted.¹⁷ Nevertheless, the sluggish water dissociation into H^+ and OH^- inside the bipolar membrane

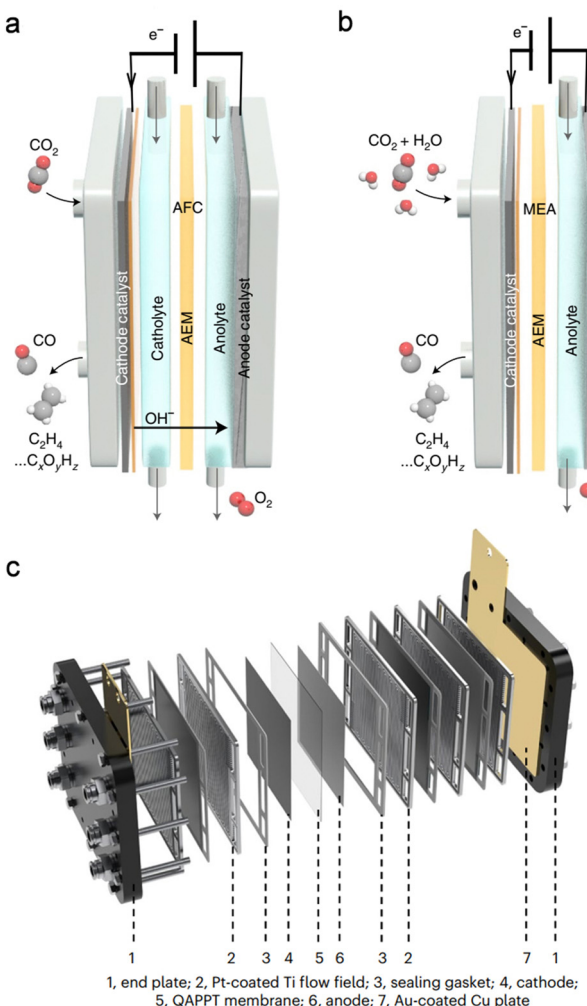


Fig. 8 Schematic of (a) an alkaline electrolyte flow cell (AFC) and (b) an MEA electrolyser. Reproduced with permission from ref. 65. Copyright 2022, Springer Nature. (c) Scale-up electrolyser stack with four $10 \times 10 \text{ cm}^2$ MEAs. Reproduced with permission from ref. 67. Copyright 2023, Springer Nature.

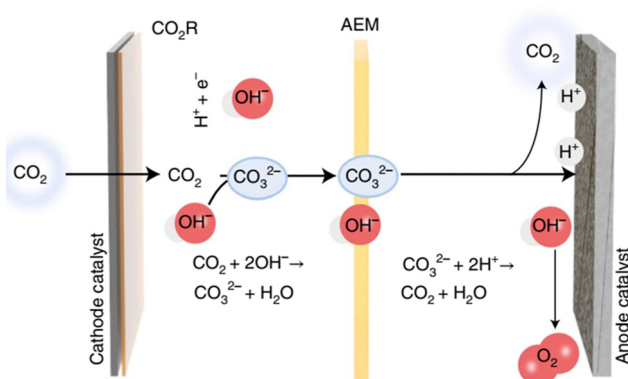


Fig. 9 CO_2 loss via carbonate formation and crossover to the anodic side under alkaline conditions. Reproduced with permission from ref. 65. Copyright 2022, Springer Nature.

as well as the increased membrane thickness leads to extra voltage loss compared with an AEM or cation exchange membrane (CEM). In addition, the higher expense of the bipolar membrane also hinders its application.

3.3. Development of an electrocatalyst under acidic conditions

As mentioned above, overall CO_2 electrolysis in acidic electrolytes can address the issue of CO_2 loss for improved energy efficiency. Although performing the CO_2RR under acidic conditions is preferred, and indeed improved performances were obtained for the acidic CO_2RR by controlling the catalyst surface microenvironments,^{68–72} few catalysts have shown promising activity for the alternative anodic reactions in acidic anolyte. In fact, the hydroxyl group ($^*\text{OH}$) plays a pivotal role in the dehydrogenation processes of the anodic oxidation reactions, the formation of which is hindered due to the acidic conditions.⁷³ Moreover, operation at the positive potential in an acidic solution will cause rapid decomposition of the non-noble metal anode, resulting in poor stability. A recent work presented an electrocatalyst featuring MnO_2 nanosheets for the acidic GOR.⁷⁴ A long-term steady electrolysis of over 800 h was achieved at 10 mA cm^{-2} in 0.2 M glycerol + 0.005 M H_2SO_4 . However, both formate and CO_2 were obtained with close FEs ($\sim 50\%$ for each), indicating the easy overoxidation of glycerol under acidic conditions. Therefore, developing highly acid-tolerant electrocatalysts with enhanced activity and selectivity remains a great challenge, and demands further investigations.

3.4. Selectivity control for target products

It is quite challenging to control the selectivity of certain products for anodic organic oxidations. For instance, in alcohol oxidations, the C–OH group easily gets oxidized to –COOH rather than –CHO. Therefore, partial oxidation of alcohol to aldehyde is difficult. It becomes more challenging to selectively produce intermediate chemicals when there are more than one reductive group in the reactant molecule. For the HMFOR, owing to the coexistence of –CHO and – CH_2OH groups in an HMF molecule, the oxidation of HMF to FDCA can proceed via

HMFCA or DFF (Fig. 6). However, given the widely-used alkaline electrolyte for the HMFOR in the CO_2RR –HMFOR couple, the HMFCA pathway is usually preferred and thus it is difficult to obtain DFF in such a coupling system.⁴⁶ Besides, C–C bond breaking may occur under harsh conditions for multi-carbon molecules, increasing the variety of products.¹⁹ Moreover, over-oxidation of organic molecules to CO_2 was also observed at high potentials/current densities. For example, quite an amount of CO_2 can be generated during the MOR on Pt and IrO_2 catalysts at $\sim 100 \text{ mA cm}^{-2}$.¹⁵ Simultaneously achieving high current density and selectivity in these alternative organic oxidation reactions remains challenging. As for the cathodic side, although most works show no significant change in the selectivity of the CO_2RR when the CO_2RR is coupled with alternative anodic oxidation reactions, sometimes the organic molecules may cross the ion-exchange membrane to the cathodic side and influence the CO_2RR process.

4. Conclusions and perspectives

Coupling CO_2RR to various anodic oxidation reactions with value-added products provides a novel avenue for enhancing the economic output of overall CO_2 electrolysis. In this review, a series of oxidation reactions have been discussed as competing alternatives to the OER with reference to the latest advances. We have also pointed out the major challenges in achieving efficient overall CO_2 electrolysis with alternative anodic reactions. Despite the pronounced advancement made in the coupling strategy, this field is still nascent.

The design of efficient electrocatalysts requires an in-depth understanding of the mechanisms, which largely relies on advanced characterization studies and theoretical simulations.⁷⁵ Recently, *in situ* infrared spectroscopy, X-ray photo-electron spectroscopy (XPS), X-ray absorption fine structure spectroscopy and other techniques have been adopted in many works, providing useful local information about reaction intermediates. However, given the complex microenvironment over the catalyst's surface during the reaction, detecting the evolution of active sites and intermediates under working conditions using operando characterization is crucial to uncover the true reaction pathways, which is still difficult owing to the harsh conditions such as high vacuum for XPS and the severe decay and disturbance of signals by the electrolyte for infrared spectroscopy.^{76,77} The design of electrolyzers that are compatible to various operando and time-resolved characterization studies is in urgent demand.

As for theoretical simulation, the accuracy of the model directly influences the calculation result, which is, however, extremely challenging in heterogeneous electrocatalysis considering the interfacial diversity. The structures of active sites are not uniform over the catalyst surface. Moreover, the active sites may evolve during catalysis, making it more difficult to obtain accurate surface structures for the simulation. Besides, the electrolyte near the electrode should also be taken into account in the simulation. The ion concentration and solvation

effect may influence the adsorption of intermediates, thus leading to different calculation results. Obviously, combining advanced calculation methods with operando characterization holds the key to deciphering the in-depth reaction mechanisms, and therefore benefits the development of high-performance electrocatalysts.

Beyond the catalysts, the overall design of the whole electrolysis system is also crucial, which has not received enough attention currently. For electrolyzers, the flow fields for both the anode and cathode should be specially designed to achieve efficient mass transfer. Besides, the feeding rates for CO_2 and anodic reactants should be well adjusted to optimize the total conversion rates. In addition, for industrial applications, the feeding, collecting, and recycling systems should match with each other for steady operation. A well-established overall CO_2 electrolysis system with comprehensive techno-economic evaluations requires scientists from various backgrounds including chemistry, materials science, physics, engineering, economics, etc. It is expected that continuous efforts will propel this technique to industrial application in the near future.

Author contributions

Y. L. and T. L. supervised the project. Y. L. wrote the manuscript.

Conflicts of interest

There are no conflicts to declare.

Acknowledgements

This work was supported by the National Key R & D Program of China (2017YFA0700104), the National Natural Science Foundation of China (21905204 and 21931007), and the 111 Project of China (D17003).

References

- 1 C. Chen, J. F. Khosrowabadi Kotyk and S. W. Sheehan, Progress toward commercial application of electrochemical carbon dioxide reduction, *Chem.*, 2018, **4**, 2571–2586.
- 2 R. Francke, B. Schille and M. Roemelt, Homogeneously catalyzed electroreduction of carbon dioxide—methods, mechanisms, and catalysts, *Chem. Rev.*, 2018, **118**, 4631–4701.
- 3 P. Zhu, C. Xia, C.-Y. Liu, K. Jiang, G. Gao, X. Zhang, Y. Xia, Y. Lei, H. N. Alshareef, T. P. Senftle and H. Wang, Direct and continuous generation of pure acetic acid solutions via electrocatalytic carbon monoxide reduction, *Proc. Natl. Acad. Sci. U. S. A.*, 2021, **118**, e2010868118.
- 4 J. Gu, C.-S. Hsu, L. Bai, H. M. Chen and X. Hu, Atomically dispersed Fe^{3+} sites catalyze efficient CO_2 electroreduction to CO , *Science*, 2019, **364**, 1091–1094.
- 5 J. Na, B. Seo, J. Kim, C. W. Lee, H. Lee, Y. J. Hwang, B. K. Min, D. K. Lee, H.-S. Oh and U. Lee, General techno-economic analysis for electrochemical coproduction coupling carbon dioxide reduction with organic oxidation, *Nat. Commun.*, 2019, **10**, 5193.
- 6 M.-Y. Qi, M. Conte, M. Anpo, Z.-R. Tang and Y.-J. Xu, Cooperative coupling of oxidative organic synthesis and hydrogen production over semiconductor-based photocatalysts, *Chem. Rev.*, 2021, **121**, 13051–13085.
- 7 L. Yuan, M.-Y. Qi, Z.-R. Tang and Y.-J. Xu, Coupling strategy for CO_2 valorization integrated with organic synthesis by heterogeneous photocatalysis, *Angew. Chem., Int. Ed.*, 2021, **60**, 21150–21172.
- 8 M.-Y. Qi, M. Conte, Z.-R. Tang and Y.-J. Xu, Engineering semiconductor quantum dots for selectivity switch on high-performance heterogeneous coupling photosynthesis, *ACS Nano*, 2022, **16**, 17444–17453.
- 9 F.-K. Shang, Y.-H. Li, M.-Y. Qi, Z.-R. Tang and Y.-J. Xu, Photocatalytic materials for sustainable chemistry via cooperative photoredox catalysis, *Catal. Today*, 2023, **410**, 85–101.
- 10 Y. Zhu, J. Zhang, Q. Qian, Y. Li, Z. Li, Y. Liu, C. Xiao, G. Zhang and Y. Xie, Dual nanoislands on Ni/C hybrid nanosheet activate superior hydrazine oxidation-assisted high-efficiency H_2 production, *Angew. Chem., Int. Ed.*, 2022, **61**, e202113082.
- 11 L. Zhu, J. Huang, G. Meng, T. Wu, C. Chen, H. Tian, Y. Chen, F. Kong, Z. Chang, X. Cui and J. Shi, Active site recovery and N–N bond breakage during hydrazine oxidation boosting the electrochemical hydrogen production, *Nat. Commun.*, 2023, **14**, 1997.
- 12 H. Jiang, M. Sun, S. Wu, B. Huang, C.-S. Lee and W. Zhang, Oxygen-incorporated NiMoP nanotube arrays as efficient bifunctional electrocatalysts for urea-assisted energy-saving hydrogen production in alkaline electrolyte, *Adv. Funct. Mater.*, 2021, **31**, 2104951.
- 13 S.-S. Liu, Q.-J. Xing, Y. Chen, M. Zhu, X.-H. Jiang, S.-H. Wu, W. Dai and J.-P. Zou, Photoelectrochemical degradation of organic pollutants using BiOBr anode coupled with simultaneous CO_2 reduction to liquid fuels via CuO cathode, *ACS Sustainable Chem. Eng.*, 2019, **7**, 1250–1259.
- 14 Q. Wang, C. Zhu, C. Wu and H. Yu, Direct synthesis of bismuth nanosheets on a gas diffusion layer as a high-performance cathode for a coupled electrochemical system capable of electroreduction of CO_2 to formate with simultaneous degradation of organic pollutants, *Electrochim. Acta*, 2019, **319**, 138–147.
- 15 Y. Li, C.-Z. Huo, H.-J. Wang, Z.-X. Ye, P.-P. Luo, X.-X. Cao and T.-B. Lu, Coupling CO_2 reduction with CH_3OH oxidation for efficient electrosynthesis of formate on hierarchical bifunctional CuSn alloy, *Nano Energy*, 2022, **98**, 107277.
- 16 X. Wei, Y. Li, L. Chen and J. Shi, Formic acid electro-synthesis by concurrent cathodic CO_2 reduction and anodic CH_3OH oxidation, *Angew. Chem., Int. Ed.*, 2021, **60**, 3148–3155.
- 17 C. Cao, D.-D. Ma, J. Jia, Q. Xu, X.-T. Wu and Q.-L. Zhu, Divergent paths, same goal: a pair-electrosynthesis tactic for

cost-efficient and exclusive formate production by metal-organic-framework-derived 2D electrocatalysts, *Adv. Mater.*, 2021, **33**, 2008631.

18 Y. Zhou, Z. Wang, W. Fang, R. Qi, Z. Wang, C. Xia, K. Lei, B. You, X. Yang, Y. Liu, W. Guo, Y. Su, S. Ding and B. Y. Xia, Modulating O-H activation of methanol oxidation on nickel-organic frameworks for overall CO₂ electrolysis, *ACS Catal.*, 2023, **13**, 2039–2046.

19 J. Bi, Q. Zhu, W. Guo, P. Li, S. Jia, J. Liu, J. Ma, J. Zhang, Z. Liu and B. Han, Simultaneous CO₂ reduction and 5-hydroxymethylfurfural oxidation to value-added products by electrocatalysis, *ACS Sustainable Chem. Eng.*, 2022, **10**, 8043–8050.

20 Y. Liang, W. Zhou, Y. Shi, C. Liu and B. Zhang, Unveiling in situ evolved In/In₂O_{3-x} heterostructure as the active phase of In₂O₃ toward efficient electroreduction of CO₂ to formate, *Sci. Bull.*, 2020, **65**, 1547–1554.

21 T. Wang, X. Cao and L. Jiao, Progress in hydrogen production coupled with electrochemical oxidation of small molecules, *Angew. Chem., Int. Ed.*, 2022, **61**, e202213328.

22 J. Jack, W. Zhu, J. L. Avalos, J. Gong and Z. J. Ren, Anode valorization for scalable and sustainable electrolysis, *Green Chem.*, 2021, **23**, 7917–7936.

23 L. Chen and J. Shi, Co-electrolysis toward value-added chemicals, *Sci. China Mater.*, 2022, **65**, 1–9.

24 S. A. Lee, M. G. Lee and H. W. Jang, Catalysts for electrochemical ammonia oxidation: Trend, challenge, and promise, *Sci. China Mater.*, 2022, **65**, 3334–3352.

25 K. Siddharth, Y. Hong, X. Qin, H. J. Lee, Y. T. Chan, S. Zhu, G. Chen, S.-I. Choi and M. Shao, Surface engineering in improving activity of Pt nanocubes for ammonia electro-oxidation reaction, *Appl. Catal., B*, 2020, **269**, 118821.

26 M. J. Trenerry, C. M. Wallen, T. R. Brown, S. V. Park and J. F. Berry, Spontaneous N₂ formation by a diruthenium complex enables electrocatalytic and aerobic oxidation of ammonia, *Nat. Chem.*, 2021, **13**, 1221–1227.

27 W. Xu, D. Du, R. Lan, J. Humphreys, D. N. Miller, M. Walker, Z. Wu, J. T. S. Irvine and S. Tao, Electrodeposited NiCu bimetal on carbon paper as stable non-noble anode for efficient electrooxidation of ammonia, *Appl. Catal., B*, 2018, **237**, 1101–1109.

28 F. Almomani, R. Bhosale, M. Khraisheh, A. Kumar and M. Tawalbeh, Electrochemical oxidation of ammonia on nickel oxide nanoparticles, *Int. J. Hydrogen Energy*, 2020, **45**, 10398–10408.

29 X. V. Medvedeva, J. J. Medvedev, S. W. Tatarchuk, R. M. Choueiri and A. Klinkova, Sustainable at both ends: electrochemical CO₂ utilization paired with electrochemical treatment of nitrogenous waste, *Green Chem.*, 2020, **22**, 4456–4462.

30 M. Choi, J. W. Kim, S. Chung, Y. Lee, S. Bong and J. Lee, Syngas production for Fischer-Tropsch process via co-electrolytic processes of CO₂ reduction and NH₃ oxidation, *Chem. Eng. J.*, 2022, **430**, 132563.

31 X. Wang, J.-P. Li, Y. Duan, J. Li, H. Wang, X. Yang and M. Gong, Electrochemical urea oxidation in different environment: From mechanism to devices, *ChemCatChem*, 2022, **14**, e202101906.

32 R. Clark, A. Moore, M. MacInnis and E. Bertin, Investigation of urea oxidation as a potential anode reaction during CO₂ electrolysis, *J. Appl. Electrochem.*, 2021, **51**, 1583–1590.

33 J.-H. Guo and W.-Y. Sun, Integrating nickel-nitrogen doped carbon catalyzed CO₂ electroreduction with chlor-alkali process for CO, Cl₂ and KHCO₃ production with enhanced techno-economics, *Appl. Catal., B*, 2020, **275**, 119154.

34 R. Ge, L.-Y. Dong, X. Hu, Y.-T. Wu, L. He, G.-P. Hao and A.-H. Lu, Intensified coupled electrolysis of CO₂ and brine over electrocatalysts with ordered mesoporous transport channels, *Chem. Eng. J.*, 2022, **438**, 135500.

35 X. Tan, C. Yu, X. Song, C. Zhao, S. Cui, H. Xu, J. Chang, W. Guo, Z. Wang, Y. Xie and J. Qiu, Toward an understanding of the enhanced CO₂ electroreduction in NaCl electrolyte over CoPc molecule-implanted graphitic carbon nitride catalyst, *Adv. Energy Mater.*, 2021, **11**, 2100075.

36 L. Fan, X. Bai, C. Xia, X. Zhang, X. Zhao, Y. Xia, Z.-Y. Wu, Y. Lu, Y. Liu and H. Wang, CO₂/carbonate-mediated electrochemical water oxidation to hydrogen peroxide, *Nat. Commun.*, 2022, **13**, 2668.

37 S.-N. Sun, L.-Z. Dong, J.-R. Li, J.-W. Shi, J. Liu, Y.-R. Wang, Q. Huang and Y.-Q. Lan, Redox-active crystalline coordination catalyst for hybrid electrocatalytic methanol oxidation and CO₂ reduction, *Angew. Chem., Int. Ed.*, 2022, **61**, e202207282.

38 S. Verma, S. Lu and P. J. A. Kenis, Co-electrolysis of CO₂ and glycerol as a pathway to carbon chemicals with improved technoeconomics due to low electricity consumption, *Nat. Energy*, 2019, **4**, 466–474.

39 K. Fernández-Caso, A. Peña-Rodríguez, J. Solla-Gullón, V. Montiel, G. Díaz-Sainz, M. Alvarez-Guerra and A. Irabien, Continuous carbon dioxide electroreduction to formate coupled with the single-pass glycerol oxidation to high value-added products, *J. CO₂ Util.*, 2023, **70**, 102431.

40 G. Wang, J. Chen, K. Li, J. Huang, Y. Huang, Y. Liu, X. Hu, B. Zhao, L. Yi, T. W. Jones and Z. Wen, Cost-effective and durable electrocatalysts for Co-electrolysis of CO₂ conversion and glycerol upgrading, *Nano Energy*, 2022, **92**, 106751.

41 M. A. Bajada, S. Roy, J. Warnan, K. Abdiaziz, A. Wagner, M. M. Roessler and E. Reisner, A precious-metal-free hybrid electrolyzer for alcohol oxidation coupled to CO₂-to-syngas conversion, *Angew. Chem., Int. Ed.*, 2020, **59**, 15633–15641.

42 G. Yang, Y. Jiao, H. Yan, Y. Xie, A. Wu, X. Dong, D. Guo, C. Tian and H. Fu, Interfacial engineering of MoO₂-FeP heterojunction for highly efficient hydrogen evolution coupled with biomass electrooxidation, *Adv. Mater.*, 2020, **32**, 2000455.

43 P. Prabhu, Y. Wan and J.-M. Lee, Electrochemical conversion of biomass derived products into high-value chemicals, *Matter*, 2020, **3**, 1162–1177.

44 K. Gu, D. Wang, C. Xie, T. Wang, G. Huang, Y. Liu, Y. Zou, L. Tao and S. Wang, Defect-rich high-entropy oxide nanosheets for efficient 5-hydroxymethylfurfural electrooxidation, *Angew. Chem., Int. Ed.*, 2021, **60**, 20253–20258.

45 R. Ge, Y. Wang, Z. Li, M. Xu, S.-M. Xu, H. Zhou, K. Ji, F. Chen, J. Zhou and H. Duan, Selective electrooxidation of biomass-derived alcohols to aldehydes in a neutral medium: Promoted water dissociation over a nickel-oxide-supported ruthenium single-atom catalyst, *Angew. Chem., Int. Ed.*, 2022, **61**, e202200211.

46 Y. Yang and T. Mu, Electrochemical oxidation of biomass derived 5-hydroxymethylfurfural (HMF): pathway, mechanism, catalysts and coupling reactions, *Green Chem.*, 2021, **23**, 4228–4254.

47 N. Zhang, Y. Zou, L. Tao, W. Chen, L. Zhou, Z. Liu, B. Zhou, G. Huang, H. Lin and S. Wang, Electrochemical oxidation of 5-hydroxymethylfurfural on nickel nitride/carbon nanosheets: Reaction pathway determined by in situ sum frequency generation vibrational spectroscopy, *Angew. Chem., Int. Ed.*, 2019, **58**, 15895–15903.

48 Y. Lu, T. Liu, Y.-C. Huang, L. Zhou, Y. Li, W. Chen, L. Yang, B. Zhou, Y. Wu, Z. Kong, Z. Huang, Y. Li, C.-L. Dong, S. Wang and Y. Zou, Integrated catalytic sites for highly efficient electrochemical oxidation of the aldehyde and hydroxyl groups in 5-hydroxymethylfurfural, *ACS Catal.*, 2022, **12**, 4242–4251.

49 K. Yang, N. Zhang, J. Yang, Z. Xu, J. Yan, D. Li and S. Liu, Synergistic marriage of CO₂ reduction and sulfide oxidation towards a sustainable co-electrolysis process, *Appl. Catal., B*, 2023, **332**, 122718.

50 J. C. Fornaciari, D. Primc, K. Kawashima, B. R. Wygant, S. Verma, L. Spanu, C. B. Mullins, A. T. Bell and A. Z. Weber, A perspective on the electrochemical oxidation of methane to methanol in membrane electrode assemblies, *ACS Energy Lett.*, 2020, **5**, 2954–2963.

51 E. Sargeant, A. Kolodziej, C. S. Le Duff and P. Rodriguez, Electrochemical conversion of CO₂ and CH₄ at subzero temperatures, *ACS Catal.*, 2020, **10**, 7464–7474.

52 J. Lu, C. Zhu, C. Pan, W. Lin, J. P. Lemmon, F. Chen, C. Li and K. Xie, Highly efficient electrochemical reforming of CH₄/CO₂ in a solid oxide electrolyser, *Sci. Adv.*, 2018, **4**, eaar5110.

53 T. Tan, W. Wang, K. Zhang, Z. Zhan, W. Deng, Q. Zhang and Y. Wang, Upcycling plastic wastes into value-added products by heterogeneous catalysis, *ChemSusChem*, 2022, **15**, e202200522.

54 X. Du, H. Zhang, K. P. Sullivan, P. Gogoi and Y. Deng, Electrochemical lignin conversion, *ChemSusChem*, 2020, **13**, 4318–4343.

55 H. Zhao, D. Lu, J. Wang, W. Tu, D. Wu, S. W. Koh, P. Gao, Z. J. Xu, S. Deng, Y. Zhou, B. You and H. Li, Raw biomass electroreforming coupled to green hydrogen generation, *Nat. Commun.*, 2021, **12**, 2008.

56 X. Du, W. Liu, Z. Zhang, A. Mulyadi, A. Brittain, J. Gong and Y. Deng, Low-energy catalytic electrolysis for simultaneous hydrogen evolution and lignin depolymerization, *ChemSusChem*, 2017, **10**, 847–854.

57 F.-Y. Chen, Z.-Y. Wu, S. Gupta, D. J. Rivera, S. V. Lambeets, S. Pecaut, J. Y. T. Kim, P. Zhu, Y. Z. Finfrock, D. M. Meira, G. King, G. Gao, W. Xu, D. A. Cullen, H. Zhou, Y. Han, D. E. Perea, C. L. Muhich and H. Wang, Efficient conversion of low-concentration nitrate sources into ammonia on a Ru-dispersed Cu nanowire electrocatalyst, *Nat. Nanotechnol.*, 2022, **17**, 759–767.

58 G. Lee, Y. C. Li, J.-Y. Kim, T. Peng, D.-H. Nam, A. Sedighian Rasouli, F. Li, M. Luo, A. H. Ip, Y.-C. Joo and E. H. Sargent, Electrochemical upgrade of CO₂ from amine capture solution, *Nat. Energy*, 2021, **6**, 46–53.

59 I. Sullivan, A. Goryachev, I. A. Digdaya, X. Li, H. A. Atwater, D. A. Vermaas and C. Xiang, Coupling electrochemical CO₂ conversion with CO₂ capture, *Nat. Catal.*, 2021, **4**, 952–958.

60 D. M. Weekes, D. A. Salvatore, A. Reyes, A. Huang and C. P. Berlinguette, Electrolytic CO₂ reduction in a flow cell, *Acc. Chem. Res.*, 2018, **51**, 910–918.

61 S. Liang, N. Altaf, L. Huang, Y. Gao and Q. Wang, Electrolytic cell design for electrochemical CO₂ reduction, *J. CO₂ Util.*, 2020, **35**, 90–105.

62 J. Li, G. Chen, Y. Zhu, Z. Liang, A. Pei, C.-L. Wu, H. Wang, H. R. Lee, K. Liu, S. Chu and Y. Cui, Efficient electrocatalytic CO₂ reduction on a three-phase interface, *Nat. Catal.*, 2018, **1**, 592–600.

63 T.-T. Zhuang, Z.-Q. Liang, A. Seifitokaldani, Y. Li, P. De Luna, T. Burdyny, F. Che, F. Meng, Y. Min, R. Quintero-Bermudez, C. T. Dinh, Y. Pang, M. Zhong, B. Zhang, J. Li, P.-N. Chen, X.-L. Zheng, H. Liang, W.-N. Ge, B.-J. Ye, D. Sinton, S.-H. Yu and E. H. Sargent, Steering post-C–C coupling selectivity enables high efficiency electroreduction of carbon dioxide to multi-carbon alcohols, *Nat. Catal.*, 2018, **1**, 421–428.

64 C.-T. Dinh, T. Burdyny, M. G. Kibria, A. Seifitokaldani, C. M. Gabardo, F. P. García de Arquer, A. Kiani, J. P. Edwards, P. De Luna, O. S. Bushuyev, C. Zou, R. Quintero-Bermudez, Y. Pang, D. Sinton and E. H. Sargent, CO₂ electroreduction to ethylene via hydroxide-mediated copper catalysis at an abrupt interface, *Science*, 2018, **360**, 783–787.

65 A. Ozden, F. P. García de Arquer, J. E. Huang, J. Wicks, J. Sisler, R. K. Miao, C. P. O'Brien, G. Lee, X. Wang, A. H. Ip, E. H. Sargent and D. Sinton, Carbon-efficient carbon dioxide electrolyzers, *Nat. Sustainable*, 2022, **5**, 563–573.

66 T. Zheng, K. Jiang, N. Ta, Y. Hu, J. Zeng, J. Liu and H. Wang, Large-scale and highly selective CO₂ electrocatalytic reduction on nickel single-atom catalyst, *Joule*, 2019, **3**, 265–278.

67 P. Wei, D. Gao, T. Liu, H. Li, J. Sang, C. Wang, R. Cai, G. Wang and X. Bao, Coverage-driven selectivity switch from ethylene to acetate in high-rate CO₂/CO electrolysis, *Nat. Nanotechnol.*, 2023, **18**, 299–306.

68 M. C. O. Monteiro, M. F. Philips, K. J. P. Schouten and M. T. M. Koper, Efficiency and selectivity of CO₂ reduction to CO on gold gas diffusion electrodes in acidic media, *Nat. Commun.*, 2021, **12**, 4943.

69 Y. Xie, P. Ou, X. Wang, Z. Xu, Y. C. Li, Z. Wang, J. E. Huang, J. Wicks, C. McCallum, N. Wang, Y. Wang, T. Chen, B. T. W. Lo, D. Sinton, J. C. Yu, Y. Wang and E. H. Sargent, High carbon utilization in CO₂ reduction to multi-carbon products in acidic media, *Nat. Catal.*, 2022, **5**, 564–570.

70 J. Gu, S. Liu, W. Ni, W. Ren, S. Haussener and X. Hu, Modulating electric field distribution by alkali cations for CO_2 electroreduction in strongly acidic medium, *Nat. Catal.*, 2022, **5**, 268–276.

71 J. E. Huang, F. Li, A. Ozden, A. Sedighian Rasouli, F. P. García de Arquer, S. Liu, S. Zhang, M. Luo, X. Wang, Y. Lum, Y. Xu, K. Bertens, R. K. Miao, C.-T. Dinh, D. Sinton and E. H. Sargent, CO_2 electrolysis to multicarbon products in strong acid, *Science*, 2021, **372**, 1074–1078.

72 Y. Zhao, L. Hao, A. Ozden, S. Liu, R. K. Miao, P. Ou, T. Alkayyali, S. Zhang, J. Ning, Y. Liang, Y. Xu, M. Fan, Y. Chen, J. E. Huang, K. Xie, J. Zhang, C. P. O'Brien, F. Li, E. H. Sargent and D. Sinton, Conversion of CO_2 to multi-carbon products in strong acid by controlling the catalyst microenvironment, *Nat. Synth.*, 2023, **2**, 403–412.

73 T. Iwasita, Electrocatalysis of methanol oxidation, *Electrochim. Acta*, 2002, **47**, 3663–3674.

74 Y. Li, X. Wei, S. Han, L. Chen and J. Shi, MnO_2 electrocatalysts coordinating alcohol oxidation for ultra-durable hydrogen and chemical productions in acidic solutions, *Angew. Chem., Int. Ed.*, 2021, **60**, 21464–21472.

75 L. Li, Y. Sun and Y. Xie, Catalysts design for CO_2 electroreduction, *Sci. China: Chem.*, 2022, **65**, 425–427.

76 Q. Liu, X.-G. Zhang, Z.-Y. Du, C.-J. Zou, H.-Y. Chen, Y. Zhao, J.-C. Dong, P.-P. Fang and J.-F. Li, Converting CO_2 to ethanol on Ag nanowires with high selectivity investigated by operando Raman spectroscopy, *Sci. China: Chem.*, 2023, **66**, 259–265.

77 X. Song, L. Xu, X. Sun and B. Han, In situ/operando characterization techniques for electrochemical CO_2 reduction, *Sci. China Chem.*, 2023, **66**, 315–323.